JOURNAL OF SOLID STATE CHEMISTRY 110, 243–249 (1994)

# Structure of $\gamma$-$Li_3AsO_4$ by High Temperature Powder Neutron Diffraction

I. Abrahams[1]

*Department of Chemistry, Queen Mary and Westfield College, University of London, Mile End Road, London E1 4NS, United Kingdom*

P. G. Bruce

*Centre for Materials and Electrochemical Sciences, Department of Chemistry, University of St. Andrews, St. Andrews, Fife KY16 9ST, United Kingdom*

W. I. F. David

*Rutherford Appleton Laboratory, SERC, Chilton, Didcot, Oxon OX11 0QX, United Kingdom*

and A. R. West

*Department of Chemistry, University of Aberdeen, Meston Walk, Old Aberdeen AB9 2UE, United Kingdom*

Received March 11, 1993; in revised form September 7, 1993; accepted September 15, 1993

The structure of $\gamma$-$Li_3AsO_4$ has been refined by Rietveld analysis of high resolution powder neutron diffraction data collected at 770 and 850°C. The structure is related to that of $\gamma$-$Li_3PO_4$, being a distorted hexagonal close-packed arrangement of oxide ions with half the tetrahedral sites filled by cations. Arsenic occupies the same sites as phosphorus in $\gamma$-$Li_3PO_4$. $Li^+$ ions show positional disorder; Li(1) ions are split into central and off-center positions within their tetrahedral sites; Li(2) ions are distributed over pairs of face sharing tetrahedral sites at 850°C while occupying only one site at 770°C. The powder neutron data show anisotropic broadening of *hkl* peaks with $h = 2n + 1$. The broadening has been accounted for using a modified Rietveld code. The broadened peaks correspond to those reflections that are not common to the related low temperature $\beta$-phase and are associated with a doubling of the *a*-axis during the $\beta$–$\gamma$ transition. The origin of the broadening is the small size of the $\gamma$-phase domains in the *a*-direction; adjacent domains are probably connected by antiphase boundaries. © 1994 Academic Press, Inc.

## INTRODUCTION

The $\gamma$-phases (1) are a group of materials which are basically isostructural with $\gamma$-$Li_3PO_4$ (2). A wide range of solid solutions containing interstitial $Li^+$ ions are obtainable based on aliovalent substitutions of stoichiometric $\gamma$-phases such as $\gamma$-$Li_2ZnSiO_4$, $\gamma$-$Li_3VO_4$, and $\gamma$-$Li_3AsO_4$ (3). Many of the interstitial solid solutions show $Li^+$ ion conductivities as high as 0.1 $\Omega^{-1}$ $cm^{-1}$ at 300°C, the best known example of which is LISICON, $Li_{2+2x}Zn_{1-x}GeO_4$ (4).

$\gamma$-$Li_3AsO_4$ is thermodynamically stable at temperatures above 750°C, below which the related $\beta$-$Li_3AsO_4$ is the stable form. In many other $\gamma$-phases the kinetics of $\gamma$–$\beta$ phase transition on cooling are slow and $\gamma$-phases may be isolated at room temperature by rapid quenching, despite being metastable with respect to the $\beta$-phases at these temperatures. In $Li_3AsO_4$ however, the $\gamma$–$\beta$ transition is so rapid that pure $\gamma$-phase samples are difficult to prepare free from $\beta$-phase using quenching techniques. A mechanism for the $\beta$–$\gamma$ phase transition has been proposed earlier (5–7). The transition essentially involves a redistribution of cations and a slight buckling of the hcp oxide layers. An alternative mechanism for the phase transition in $NaFeO_2$ has been proposed (8) which involves rotation of $FeO_4$ tetrahedra by relocation of oxide ions.

Evidence from neutron diffraction studies on $\gamma$-phase interstitial solid solutions has shown that the presence of ions in interstitial octahedral sites causes displacement of ions from neighboring tetrahedral sites in order to minimize interion repulsions. Ionic conduction in these systems is believed to involve the interstitial octahedral and tetrahedral ions moving together in defect clusters (9, 10). A detailed knowledge of the $Li^+$ ion distribution is therefore important in any discussion of ionic conduction in these systems. The extra sensitivity of neutron diffraction to $Li^+$ ions when compared to the related X-ray

[1] To whom correspondence should be addressed.



0022-4596/94 $6.00
Copyright © 1994 by Academic Press, Inc.
All rights of reproduction in any form reserved.

methods allows for accurate refinement of lithium positional and occupancy parameters, within the well-characterized $\gamma$-phase framework. The structure refinement of $\gamma$-$Li_3AsO_4$ from powder neutron data is presented here.

## EXPERIMENTAL

### *Preparation*

$\beta$-$Li_3AsO_4$ was prepared by standard solid state techniques. Appropriate molar quantities of $^7Li_2CO_3$ and $As_2O_5$ were first ground together as a slurry in ethanol. After drying, the mixture was heated in a gold crucible successively for 4 hr at 650°C to drive off $CO_2$, 6 hr at 750°C, and 1 hr at 900°C to complete the reaction. After it was reground, the sample was further heated for 3 hr at 700°C to ensure complete conversion to the $\beta$-phase. Phase purity was determined by X-ray powder diffraction using a Stöe Guinier camera.

### *Data Collection*

Time-of-flight powder neutron diffraction data were collected on the HRPD diffractometer at ISIS, Rutherford Appleton Laboratory. Approximately 10 g of powdered $\beta$-$Li_3AsO_4$ was loaded into a 12-mm-diameter vanadium can and the sample placed in a furnace assembly 1 m in front of the backscattering detectors. Data were collected in the t.o.f. range 20–120 msec at 770 and 850°C. Profile plots were generated using GENIE (11) and structural projections were generated using STRUPLO (12) and PLUTO (13).

### *Structure Refinement*

A starting model based on the structure of $\gamma$-$Li_3PO_4$ was used as a basis for refinement. Refinements for both data sets were carried out in a similar way. For the 850°C data, refinement proceeded in the orthorhombic space group *Pnma* (no. 62) (14) with cell parameters derived from refinement of the *d*-spacings of 15 assigned reflections measured on the diffraction profile. Initially, a standard Rietveld refinement was carried out using the program REFINE (15) with peak shapes modeled by a convolution of pseudo-Voigt and two exponential functions. The scattering lengths used were As = 0.658, O = 0.5805, and $^7Li = -0.220 \times 10^{-12}$ cm (16). The scale and five polynomial background parameters were refined first, followed in subsequent iterations by unit cell, zero point, and peak shape parameters. Atomic and thermal parameters were also refined at this stage, but the fit remained poor with $\chi^2 = 2.84$. Close examination of the difference profile revealed large differences in *hkl* peaks with $h = 2n + 1$, which appeared broadened with respect to the other peaks. Comparison with the pattern for the $\beta$-phase showed the unbroadened peaks to be common to both $\beta$- and $\gamma$-phases while those which appear only in the $\gamma$-phase are broadened (Fig. 1).

A version of the refinement code was therefore constructed with additional Gaussian and Lorentzian peak

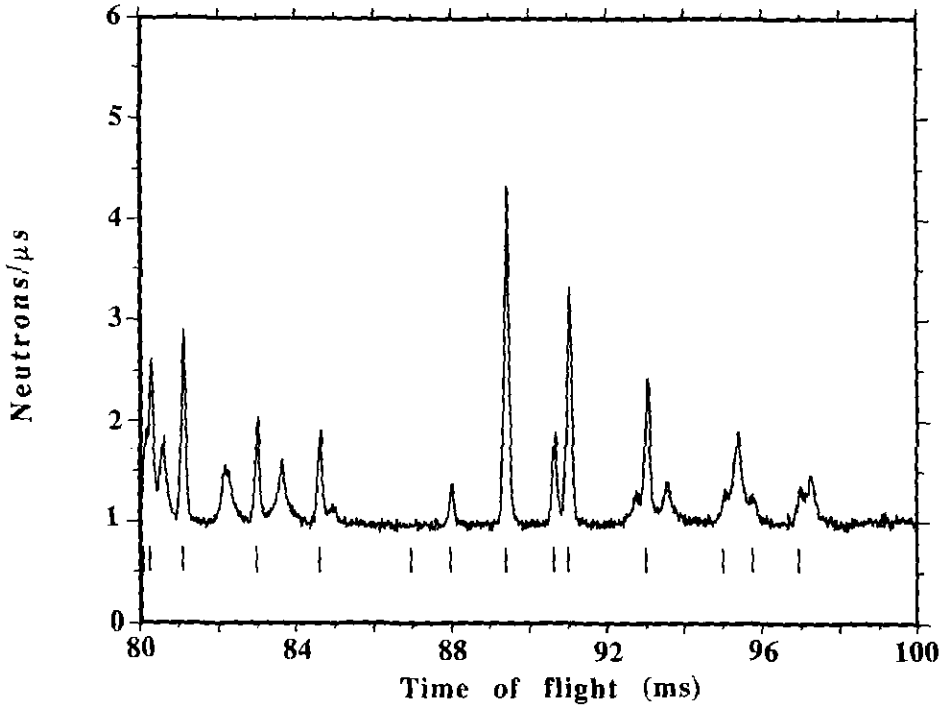


FIG. 1. Part of HRPD diffraction profile for $\gamma$-$Li_3AsO_4$, with the positions of reflections common to $\beta$-$Li_3AsO_4$ indicated by markers.

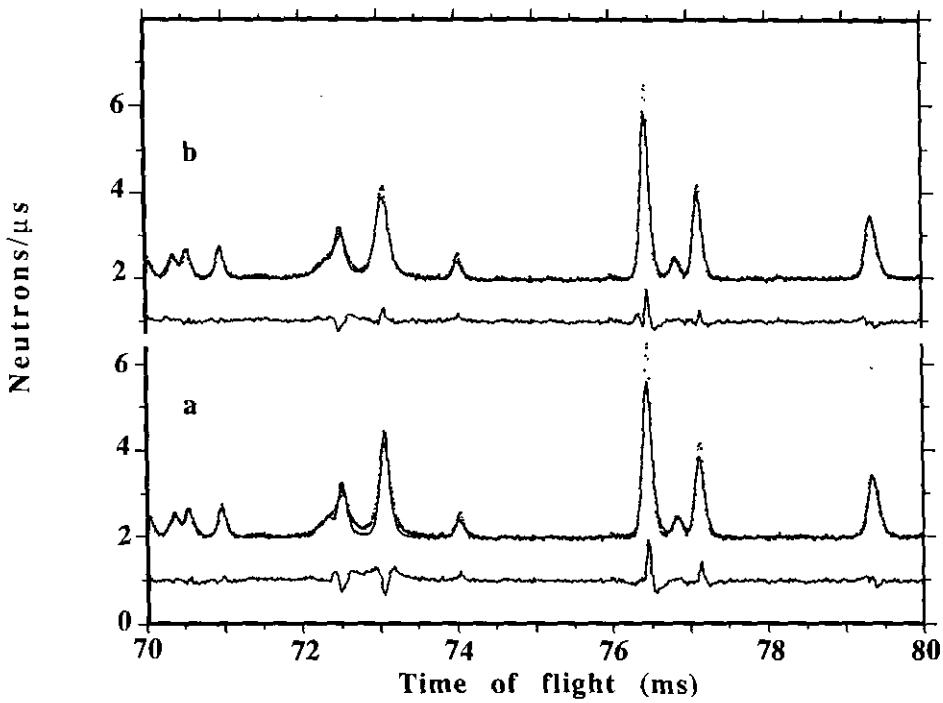


FIG. 2. Fit to $\gamma$-$Li_3AsO_4$ at 850°C using (a) standard peak shape and (b) peak shape incorporating anisotropic broadening term.

parameters for the broadened reflections. This resulted in a significantly better approximation to the profile, especially in the *hkl* broadened peaks (Fig. 2), and refinement was continued using this code.

Refinement of atomic and isotropic thermal parameters revealed high values for the lithium ions, which indicated positional as well as thermal disorder. Refinement of anisotropic thermal parameters suggested that this disorder occurs mainly in the *c*-direction. The $Li^+$ ions were therefore allowed to refine over more than one position. A second position close to Li(2) but shifted away from it in the *c*-direction was allowed to refine with lithium occupancy varying between the two positions Li(2) and Li(2*a*) and the total occupancy fixed at unity. Isotropic thermal parameters were tied for these two positions. Similarly, a position Li(1*a*) was refined close to Li(1). At 770°C only one Li(2) site refined satisfactorily. Anisotropic thermal parameters were refined for As and O atoms in both refinements and additionally for Li(2) at 770°C. The final refinements terminated with $R_{wp}$ = 3.79%, $R_{ex}$ = 2.92% and $R_{wp}$ = 4.77%, $R_{ex}$ = 4.78% for the 850 and 770°C refinements, respectively. The final refined atomic parameters are given in Tables 1a and 1b, and the final fitted profiles are shown in Figs. 3a and 3b.

## DISCUSSION

The structure of $\gamma$-$Li_3AsO_4$ is related to that of $\gamma$-$Li_3PO_4$ and consists of a distorted hexagonal close-packed array of oxide ions with cations in half the tetrahedral sites. A detailed description of the structure of $\gamma$-$Li_3AsO_4$ is aided by first considering an idealized model based on the room temperature structure of $\gamma$-$Li_3PO_4$ (2). In the idealized structure, one set of tetrahedral sites is fully occupied, with neighboring face-sharing tetrahedral remaining vacant. $AsO_4$ tetrahedra are isolated from each other and only corner share with groups of three edge-sharing $LiO_4$ tetrahedra (Fig. 4).

The true $Li^+$ ion distribution in $\gamma$-$Li_3AsO_4$ at elevated temperatures is somewhat different from the idealized model (see Fig. 5). At 850°C, $Li^+$ ions are located in four positions within the structure; two have regular tetrahedral geometry and correspond to the sites occupied in the idealized structure; the other two lithium positions represent displacements from these "ideal" locations. Li(1*a*) is a displacement of Li(1) in a direction parallel to the *c*-axis toward an empty face sharing site. Li(1*a*) in fact lies virtually within the shared O(1)–O(2)–O(3) face between the two tetrahedral sites, with three short bonds to oxygen ranging from 1.96 to 2.01 Å and two longer contacts at 2.40 and 2.80 Å to the apical oxygens. The Li(1)–Li(1*a*) contact distance of 0.50 Å is much too short to permit simultaneous occupation of both these positions. Li(2*a*) similarly represents a displacement of Li(2) away from its "parent" tetrahedral site. In this case, the displacement continues through the shared face into the neighboring tetrahedral site, so that the two ions are located within different tetrahedral sites. The interion con-

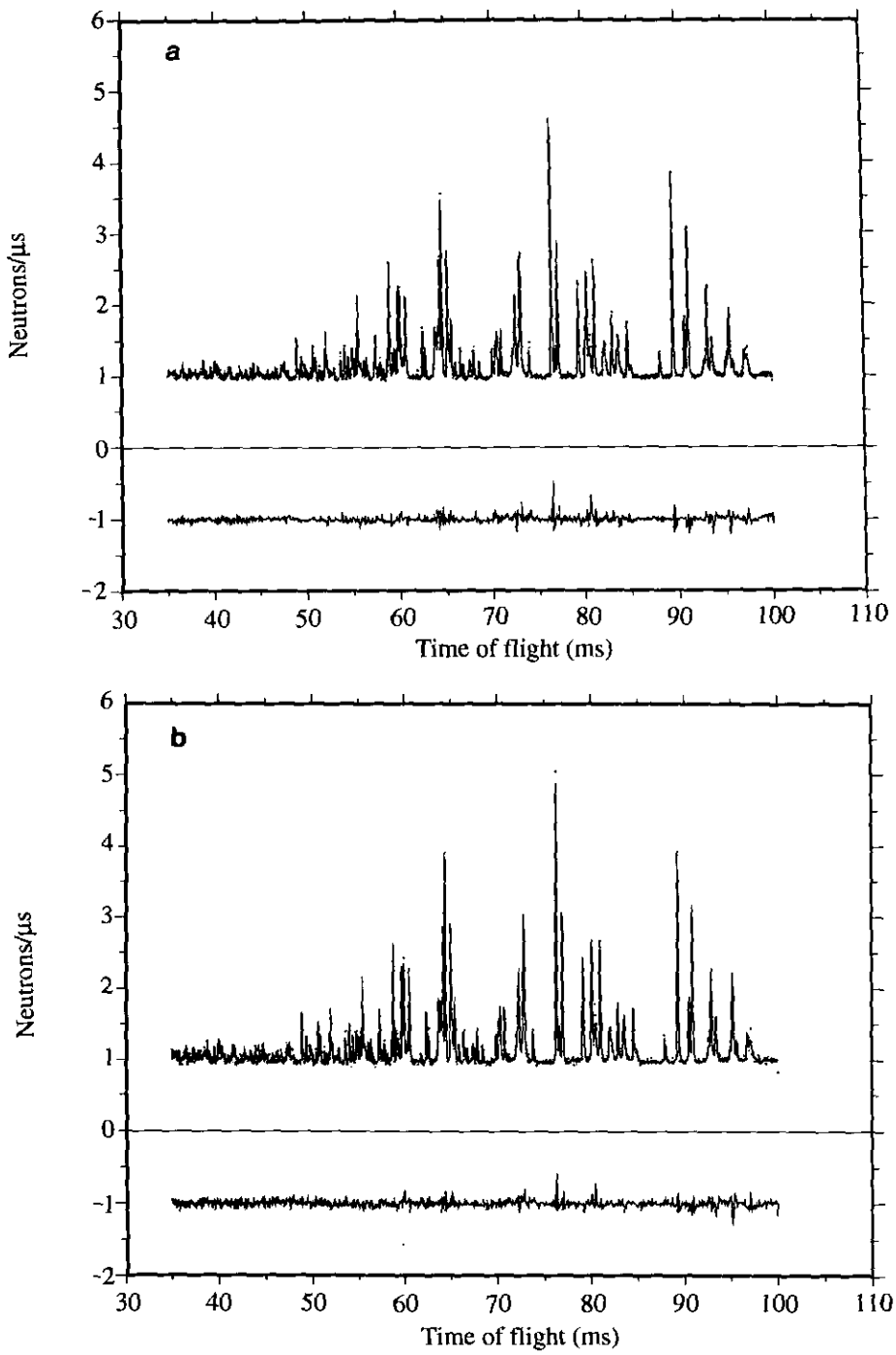


FIG. 3. Final fitted profiles for $\gamma$-$Li_3AsO_4$ at (a) 850°C and (b) 770°C. Observed (points) calculated (line) and difference (lower) profiles are shown.

tact distance of 0.76 Å again excludes simultaneous occupancy of any pair of such sites.

The type of displacement seen in the structure of $\gamma$-$Li_3AsO_4$ is not unique. The structures of $\gamma$-$Li_3Zn_{0.5}GeO_4$ (17) and $\gamma$-$Li_{3.5}Ge_{0.5}V_{0.5}O_4$ (18) also show similar displacements of $Li^+$ ions. However, in these systems the displacements are correlated with the presence of interstitial $Li^+$ ions in neighboring octahedral sites. No such relationship is evident in the structure of $\gamma$-$Li_3AsO_4$. The displacement of $Li^+$ ions seen in $\gamma$-$Li_3AsO_4$ reflects the physical changes that must occur during the $\beta$–$\gamma$ phase transition. In the $\beta$-phase a low energy corner sharing configuration is adopted within the hcp oxide framework (19) (Fig. 6a). Above 750°C, Li(1) is forced into an edge sharing configu-

TABLE 1a
Refined Atomic Parameters for $\gamma$-$Li_3AsO_4$ at 850°C with esd's in Parentheses

$R_{wp}$ = 3.79% $R_{ex}$ = 2.92% $\chi^2$ 1.69
$a$ = 10.9267(1) Å, $b$ = 6.38247(7), $c$ = 5.16243(6)

| Atom | Site | $x/a$ | $y/b$ | $z/c$ | $B_{Iso}$ | Occ |
|---|---|---|---|---|---|---|
| As | 4c | 0.4125(1) | 0.25(—) | 0.3147(3) | — | 1.0(—) |
| O(1) | 8d | 0.3392(1) | 0.0331(2) | 0.2125(3) | — | 1.0(—) |
| O(2) | 4c | 0.0562(2) | 0.25(—) | 0.2928(5) | — | 1.0(—) |
| O(3) | 4c | 0.0889(2) | 0.75(—) | 0.1424(4) | — | 1.0(—) |
| Li(1) | 4c | 0.429(1) | 0.75(—) | 0.162(6) | 2.3(1) | 0.53(5) |
| Li(1a) | 4c | 0.417(2) | 0.75(—) | 0.254(7) | 2.3(1) | 0.47(5) |
| Li(2) | 8d | 0.1649(5) | 0.5094(7) | 0.303(1) | 2.8(1) | 0.818(9) |
| Li(2a) | 8d | 0.172(2) | 0.457(3) | 0.172(5) | 2.8(1) | 0.182(9) |

Anisotropic Thermal Parameters

| | $B_{11}$ | $B_{22}$ | $B_{33}$ | $B_{23}$ | $B_{13}$ | $B_{12}$ |
|---|---|---|---|---|---|---|
| As | 1.48(6) | 1.67(7) | 1.8(1) | 0.0(—) | 0.26(7) | 0.0(—) |
| O(1) | 2.46(5) | 2.63(7) | 4.53(8) | −0.66(6) | −0.43(7) | −0.37(5) |
| O(2) | 1.54(8) | 3.16(8) | 3.6(1) | 0.0(—) | −1.77(8) | 0.0(—) |
| O(3) | 2.77(9) | 3.73(9) | 2.0(1) | 0.0(—) | 0.14(8) | 0.0(—) |

*Note*. Definition of $R$ factors:

$$R_{wp} = 100\left(\frac{\Sigma_i w_i |Y_i(\text{obs}) - Y_i(\text{calc})|^2}{\Sigma_i w_i Y_i(\text{obs})^2}\right)^{1/2}$$

$$R_{ex} = 100\left(\frac{(N - P + C)}{\Sigma_i w_i Y_i(\text{obs})^2}\right)^{1/2}$$

$$\chi^2 = \left(\frac{R_{wp}}{R_{ex}}\right)^2.$$

TABLE 1b
Refined Atomic Parameters for $\gamma$-$Li_3AsO_4$ at 770°C with esd's In Parentheses

$R_{wp}$ = 4.77% $R_{ex}$ = 4.78% $\chi^2$ = 1.00
$a$ = 10.9076(2) Å, $b$ = 6.3694(1), $c$ = 5.1488(1)

| Atom | Site | $x/a$ | $y/b$ | $z/c$ | $B_{Iso}$ | Occ |
|---|---|---|---|---|---|---|
| As | 4c | 0.4134(2) | 0.25(—) | 0.3137(4) | — | 1.0(—) |
| O(1) | 8d | 0.3396(2) | 0.0326(3) | 0.2212(4) | — | 1.0(—) |
| O(2) | 4c | 0.0562(2) | 0.25(—) | 0.2914(7) | — | 1.0(—) |
| O(3) | 4c | 0.0887(3) | 0.75(—) | 0.1438(5) | — | 1.0(—) |
| Li(1) | 4c | 0.424(3) | 0.75(—) | 0.156(14) | 2.5(2) | 0.40(9) |
| Li(1a) | 4c | 0.418(2) | 0.75(—) | 0.245(9) | 2.5(2) | 0.60(9) |
| Li(2) | 8d | 0.1645(6) | 0.5056(8) | 0.297(1) | — | 0.98(3) |

Anisotropic Thermal Parameters

| | $B_{11}$ | $B_{22}$ | $B_{33}$ | $B_{23}$ | $B_{13}$ | $B_{12}$ |
|---|---|---|---|---|---|---|
| As | 1.44(9) | 1.98(10) | 1.49(12) | 0.0(—) | 0.40(9) | 0.0(—) |
| O(1) | 2.38(7) | 2.18(8) | 4.10(10) | −0.77(8) | −0.44(9) | −0.52(7) |
| O(2) | 1.90(11) | 2.93(11) | 3.67(16) | 0.0(—) | −1.66(12) | 0.0(—) |
| O(3) | 2.60(12) | 3.15(12) | 1.62(14) | 0.0(—) | 0.17(10) | 0.0(—) |
| Li(2) | 1.10(30) | 1.05(30) | 2.28(37) | 2.23(22) | −1.37(25) | −0.64(20) |

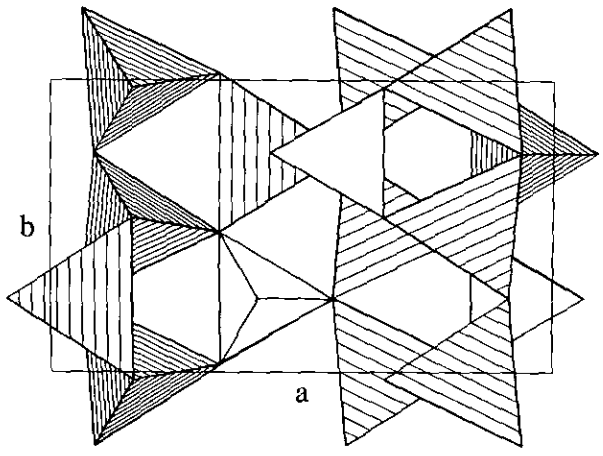


FIG. 4. Projection onto $a/b$ of the idealized structure of $\gamma$-$Li_3AsO_4$. Shaded and unshaded tetrahedra represent $LiO_4$ and $AsO_4$ units, respectively. No displaced ions are shown.

ration with neighboring Li(2) sites; this is accompanied by a buckling of the hcp oxide layers (Fig. 6b). Li(1*a*), therefore, represents a position lying between that occupied in the $\beta$-phase and the idealized $\gamma$-phase. The Li(2) position remains virtually unchanged from the $\beta$-phase, although there is some site distortion; additionally, some occupancy is lost to the neighboring Li(2*a*) position which is unoccupied in the lower temperature form.

The structure of $Li_3AsO_4$ just above the phase transition at 770°C closely resembles that at 850°C (see Table 2). The main differences lie in the occupancy of the displaced

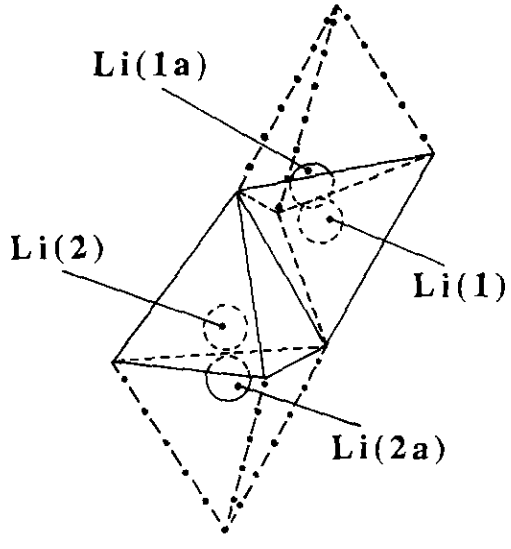


FIG. 5. Detail of $Li^+$ ion displacements in $\gamma$-$Li_3AsO_4$ at 850°C. $Li^+$ ion positions are represented by open circles within tetrahedral oxide sites. Hidden detail is shown with dashed lines, with neighboring face-sharing sites outlined using chained lines.

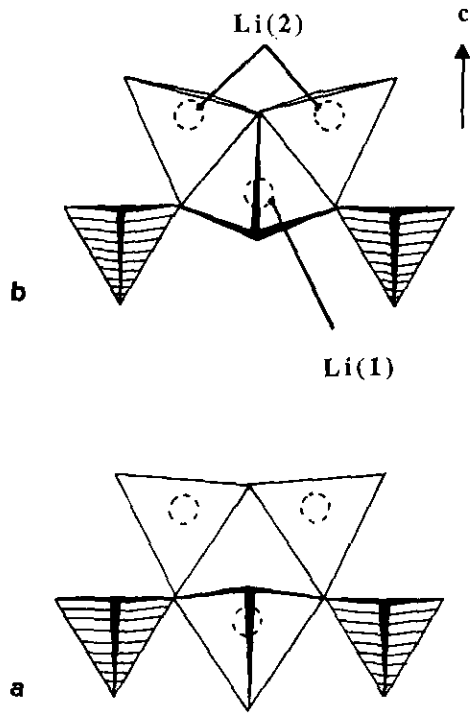


FIG. 6. Details of the $\beta$–$\gamma$ phase transition. Open and shaded tetrahedra represent $LiO_4$ and $AsO_4$ units, respectively, with dashed circles indicating $Li^+$ ion positions. (a) Part of $\beta$-phase structure showing corner sharing configuration. (b) Part of $\gamma$-phase structure showing edge-sharing configuration (note displaced ions have been omitted for clarity).

TABLE 2
Selected Interatomic Distances (Å) in $\gamma$-$Li_3AsO_4$ at 770 and 850°C, with esd's in Parentheses

| | 850°C | 770°C |
|---|---|---|
| As–O(1) | 1.684(2) ×2 | 1.686(2) ×2 |
| As–O(2) | 1.665(3) | 1.649(4) |
| As–O(3) | 1.692(3) | 1.700(3) |
| Li(1)–O(1) | 2.074(8) ×2 | 2.04(1) ×2 |
| Li(1)–O(2) | 1.91(3) | 1.89(7) |
| Li(1)–O(3) | 2.02(2) | 2.07(4) |
| Li(1a)–O(1) | 2.006(8) ×2 | 2.00(1) ×2 |
| Li(1a)–O(2) | 2.40(4) | 2.35(4) |
| Li(1a)–O(3) | 1.96(2) | 1.95(2) |
| Li(1a) ··· O(2′) | 2.80(4) | 2.83(5) |
| Li(2)–O(1) | 2.119(7) | 2.138(6) |
| Li(2)–O(1′) | 1.980(5) | 1.976(6) |
| Li(2)–O(2) | 2.038(5) | 2.011(6) |
| Li(2)–O(3) | 1.933(5) | 1.932(6) |
| Li(2a)–O(1′) | 1.84(3) | |
| Li(2a)–O(1″) | 2.43(3) | |
| Li(2a)–O(2) | 1.93(2) | |
| Li(2a)–O(3) | 2.09(2) | |
| Li(2a) ··· O(1) | 2.83(3) | |
| Li(1) ··· Li(1a) | 0.50(5) | 0.46(8) |
| Li(2) ··· Li(2a) | 0.76(3) | |

site Li(2a). At 850°C there is a significant $Li^+$ ion occupancy of both Li(2) and Li(2a) sites, while at 770°C $Li^+$ ion scattering is observed within the Li(2) site alone. Some differences are also observed in the Li(1)/Li(1a) site occupancy ratio between the two temperatures, with a higher occupancy of the Li(1a) site at 770 than at 850°C. These differences may be related to changes associated with the $\beta$–$\gamma$ transition. Certainly the difference in $Li^+$ ion distribution supports a transition mechanism involving cation relocation. However, the large thermal parameters for oxygen, particularly the $B_{33}$ parameter for O(1), might be indicative of an anion redistribution mechanism as suggested for $NaFeO_2$ (8). From these data alone it is difficult to conclude the exact nature of the $\beta$–$\gamma$ transition mechanism in $Li_3AsO_4$. It is also possible that the structure at 770°C is related to that of a transitional phase which is reported to exist in this system (3).

The $\beta$–$\gamma$ transition is characterized by a doubling in size of the unit cell along $a$ ($\beta$-$Li_3AsO_4$: $a$ = 5.4567(2), $b$ = 6.28765(2), $c$ = 5.10125(2) Å (19)), which is accompanied by a change in space group symmetry from $Pnm2_1$ to $Pnma$, giving rise to additional peaks in the diffraction pattern. It is only these additional peaks which show broadening. This selective broadening is likely to reflect anisotropy in microdomain size and indicates a small domain width in the $a$-direction. Since all other $hkl$ reflections do not show broadening, the individual crystallites are large enough in all three dimensions not to show broadening. In the $a$-direction, therefore, crystallites contain a large number of small domains with the small domain size responsible for the line broadening. It is suggested that domain boundaries are antiphase in character. A plausible displacement vector of $0.5c$ in the cation positions at the boundary would permit the domains to retain continuity of the hcp oxide layers across domain boundaries.

## ACKNOWLEDGMENTS

We thank the SERC for financial support. PGB gratefully acknowledges the Royal Society for a Pickering Research Fellowship.

## REFERENCES

1. A. R. Rodger, J. Kuwano, and A. R. West, *Solid State Ionics* **15,** 185 (1985).
2. J. Zeman, *Acta Crystallogr.* **13,** 863 (1960).
3. A. R. West and F. P. Glasser, *J. Solid State Chem.* **4,** 20 (1972).
4. H. Y-P. Hong, *Mater. Res. Bull.* **13,** 117 (1978).
5. A. R. West, *Z. Kristallogr.* **141,** 422 (1975).
6. M. E. Villafuerte-Castrejon and A. R. West, *J. Chem. Soc. Faraday Trans. 1* **75,** 374 (1979).
7. M. E. Villafuerte-Castrejon and A. R. West, *J. Chem. Soc. Faraday Trans. 1* **77,** 2297 (1981).
8. I. E. Grey, R. J. Hill, and A. W. Hewat, *Z. Kristallogr.* **193,** 51 (1990).
9. I. Abrahams and P. G. Bruce, *Philos. Mag. A* **64,** 1113 (1991).
10. P. G. Bruce and I. Abrahams, *J. Solid State Chem.* **95,** 74 (1991).

11. W. I. F. David, M. W. Johnson, K. J. Knowles, C. M. Moreton-Smith, G. D. Crosbie, E. P. Campbell, S. P. Graham, and J. S. Lyall, "GENIE—A Language for Spectral Manipulation and Display." Rutherford Appleton Laboratory, 1986.
12. R. X. Fischer, *J. Appl. Crystallogr.* **18,** 258 (1985).
13. W. D. S. Motherwell, "PLUTO—A Program for Plotting Molecular and Crystal Structures." University of Cambridge, 1979.
14. "International Tables for Crystallography, Vol. A" (Kluwer, Dordrecht, 1983.
15. W. I. F. David, "REFINE." Rutherford Appleton Laboratory, 1990.
16. L. Koester and H. Rauch, International Atomic Energy Agency, Report 2517/RB (1981).
17. I. Abrahams, P. G. Bruce, W. I. F. David, and A. R. West, *Acta Crystallogr. Sect. B* **45,** 457 (1989).
18. I. Abrahams and P. G. Bruce, *Acta Crystallogr. Sect. B* **47,** 696 (1991).
19. I. Abrahams and P. G. Bruce, unpublished work.